PNAS
www.pnas.org

Supplementary Information for

Local lattice distortions and dynamics in extremely overdoped superconducting $YSr_2Cu_{2.75}Mo_{0.25}O_{7.54}$

Steven D. Conradson, Theodore H. Geballe, Andrea Gauzzi, Maarit Karppinen, Changqing Jin, Gianguido Baldinozzi, Wenmin Li, Lipeng Cao, Edmondo Gilioli, Jack M. Jiang, Matthew J. Latimer, Oliver Mueller, Venera Nasretdinova

Theodore H. Geballe
Email: geballe@stanford.edu
Steven D. Conradson
Email: st3v3n.c0nrads0n@icloud.com

This PDF file includes:

www.pnas.org/cgi/doi/10.1073/pnas.1918704117

Materials and Methods. $YSr_2Cu_{2.75}Mo_{0.25}O_{7.54}$ was the same sample as in the previous report[1] Stoichiometric quantities of Y_2O_3, CuO, $SrCO_3$, and MoO_3 were dissolved in 1M HBO_3 solution. A gel was formed by adding citric acid and ethylene glycol followed by heating at 200° C. The dried, powdered gel was calcined at 600° C for 12 h. This material was ground, pressed into a pellet, and annealed at 980° C for 24 h twice. This material was mixed with 35 mol % $KClO_3$ and then heated to 500° C mixture at 4 GPa. The $YSr_2Cu_{2.75}Mo_{0.25}O_{7.54}$ composition was determined by Rietveld refinement neutron diffraction data. A substantial O and corresponding charge excess using this method have been verified by XAS measurements[2]. In addition to the desired product, the sample contained 4.5% KCl (4.5 %) and 0.5% remaining $KClO_3$. Other impurity concentrations are less than 1%. Susceptibility and other measurements have been presented in [3].

For these XAFS measurements, the original sample from [1] was reannealed to give the same T_c, superconducting fraction, and other properties as before although with a somewhat broader transition[3]. Atom labels are the same as used previously. The material was ground with a mortar and pestle, suspended in epoxy, and the epoxy allowed to set and cure in the bore of a 12 T magnet at Universite Pierre et Marie Curie. XRD analysis shows only the diffraction pattern of $YSr_2Cu_{2.75}Mo_{0.25}O_{7.54}$ and the essentially complete cylindrical orientation of the YSCO-Mo along the *c* axis coincident with the applied field. Its behavior is therefore identical with all other cuprates (except $Sr_sCuO_{3.3}$[4]), giving E||*c* and E⊥*c*||*aa* (in the *aa* plane) spectra.

This orientation method is common to most or all XAFS studies of oriented cuprates and related materials[5-10]. Diffraction patterns of the oriented samples show, as we do here, no substantial broadening of peaks and no new ones that would be indicative of decomposition. Although more extreme, motorized methods of reducing particle sizes, e.g., ball milling are known to affect sample integrity, hand grinding with a mortar and pestle does not raise the temperature or induce shock in materials and is considered non-damaging. With the exception of $Ba_2CuO_{3+\delta}$ that is highly air sensitive, other cuprates including overdoped ones have not been reported to have such sensitivity. Temperature dependence studies show the temperatures and extents of the transitions are unaffected. Based on these precedents and the various measurements we will presume that the materials have remained sufficiently intact to produce XAFS results indicative of their true structures and properties. XAFS measurements at 62 K were performed at the Stanford Synchrotron Radiation Lightsource on beam line 2-2 in the continuous scanning mode. Transmission data were analyzed by standard methods, with one recent description in [11]. The data ranges and other specific parameters are found in the text or figures. The Cu-Cu pairs were fit with the amplitude and phase of the EXAFS wave of a ~180° Cu-O-Cu unit that is modified by the multiple scattering contributions involving the bridging O, i.e., the three and four leg paths that are enhanced by the intervening O atom. Cu-Cu pairs without bridging O are not detected, presumably because their uncorrelated thermal motion makes their EXAFS small or negligible. This is typical of unbridged pairs, such as those on the *c* axis between adjacent CuO_2 planes as shown in the main text and in the other cited studies. The 3.22 and 3.35 Å Cu-Sr distances for E||H and corresponding 3.24 and 3.38 Å distances for E⊥H are equal within the uncertainty for the two orientations. The 0.13-0.14 Å separation between the two Sr shells is just above the 0.11 Å resolution limit of these data. These results imply a single peaked but broad, anharmonic, non-Gaussian Cu-Sr distribution. Anomalous Sr distributions have been reported in other cuprates[12]. XRD data were obtained on powder diffractometers at IOP-CAS and the CEA Saclay laboratory.

Capabilities and limitations of EXAFS. The interpretation of $\chi(R)$, the Fourier transform of $\chi(k)$, in terms of the partial pair distribution function is subject to three caveats: 1) the peak positions are 0.1-0.4 Å lower than the actual distance because of the phase shift; 2) interference between overlapping peaks reduces their overall amplitude and modifies their shapes; 3) the peak width is not the actual width of the pair distribution but is determined by the relatively short range and limited number of cycles of the spectrum being transformed by an integration that spans negative to positive infinity. The extra frequencies causing the broadening of the peaks are not in the $\chi(\mathbf{k})$ data but are artifacts of the transformation that do not affect the analysis. The actual resolution, or ability to isolate signals, is $\Delta R=\pi/2k_{max}$. The beat between the signals from pairs of Cu-O shells at 1.83/2.00 or 1.92/2.09 Å occurs at k=9.2 $Å^{-1}$, well within the resolution limit of these spectra that

extend to 14.3 $Å^{-1}$. Facilitating the visualization of the behavior of specific shells of interest by subtracting the contributions of others that may have overlapping moduli but are separated by more than the resolution limit is therefore not overdetermination or other abuse of the data, especially insofar as the actual analysis is performed on $\chi(k)$ and not $\chi(R)$. The precision of EXAFS in terms of its ability to extract relevant information therefore has two areas of application. When used to determine structural parameters for a single sample the dependence of the phase shift and amplitude function on the chemical speciation of the target element and experimental errors result in uncertainties in the numbers of atoms of up to 1/3 and in the Debye-Waller factors by even larger amounts. This is especially true in disordered materials or samples where destructive interference between the EXAFS waves from the neighbor atoms causes substantial reduction in their amplitudes. However, when used as in these experiments to probe *changes* in the element specific local structures with the same or closely related samples using the same or very similar instrumentation and monochromator-detector geometries its precision can be very high, well under 0.01 Å in distances and few percent in the amplitude parameters of numbers of atoms, Debye-Waller factors, and anharmonicity or other properties of the distribution.

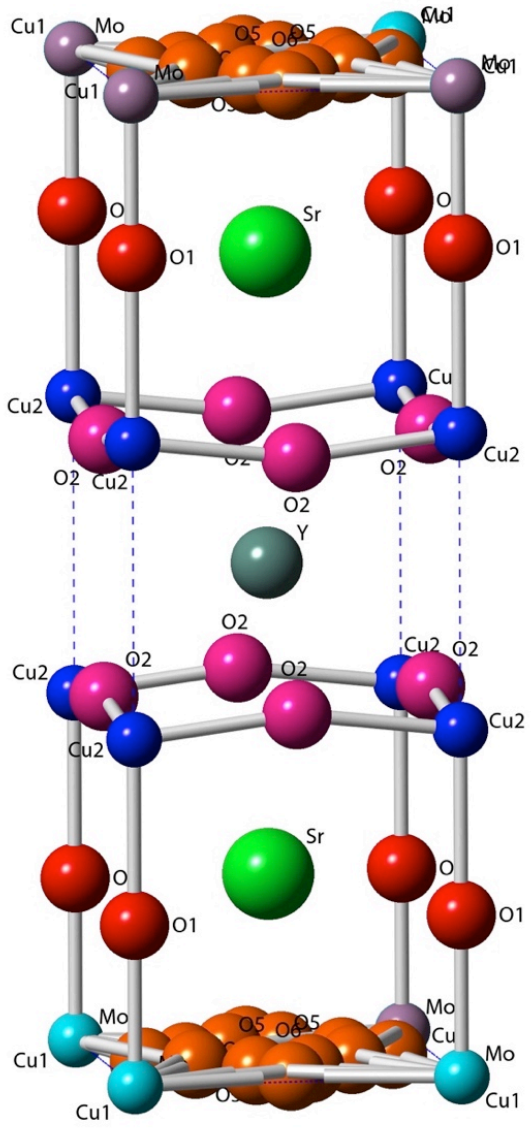

Figure S1. Unit cell of YSCO-Mo from Gauzzi et al. [1], showing labeling scheme and disorder in O4/O5 positions. In this structure the Mo and Cu1 atoms exhibit random, isomorphic placement on the Cu1/Mo sites and the O5 and O6 sites are all partially occupied. This same labeling scheme is used throughout the manuscript, except that O1 is also referred to as “Oap” and O5 and O6 are omitted with all O atoms in the Cu1-Mo plane named “O4”.

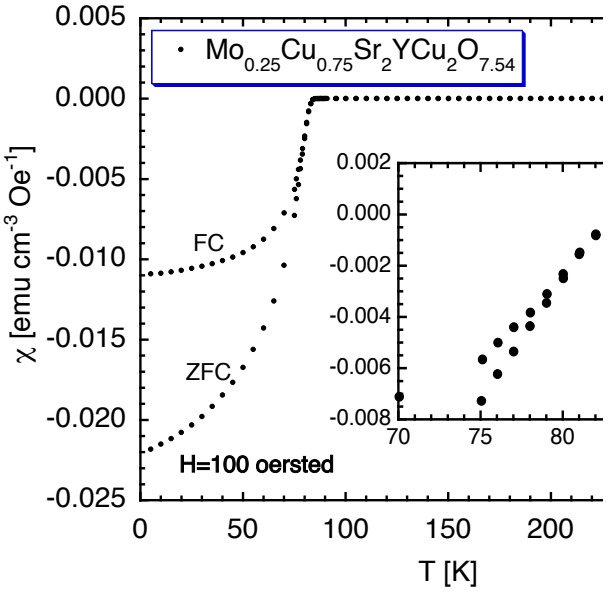

Figure S2. The XAFS sample was characterized by the same measurements as in Figure 1 of the original report of YSCO-Mo of Gauzzi et al.[1]. These are the zero-field and field-cooled (ZFC, FC) magnetization and ac susceptibility of the sample of HPO YSCO-Mo used for the XAFS measurements before it was embedded in epoxy. The inset shows an expansion of the transition below T_c. The values are close to those in the original report, demonstrating identical or very similar overall properties.

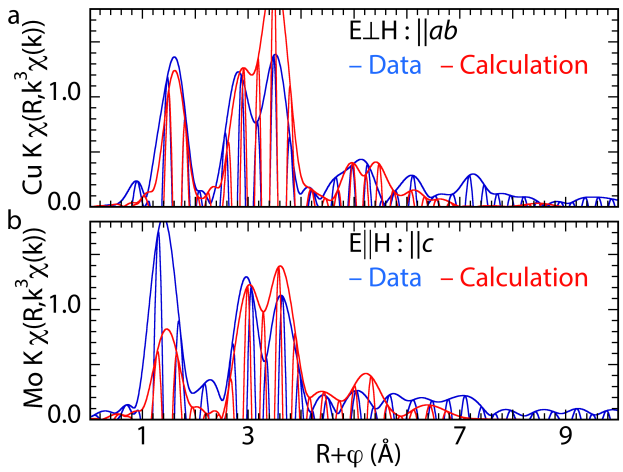

Figure S3. EXAFS (Fourier transform or χ(R) representation) of the spectrum calculated by FEFF9[13] from the crystal structure and experimentally measured YSCO-Mo a) For the Cu in the crystallographic *aa* direction. b) For the Mo measured in the *c* direction.

Although χ(R) conforms to the crystal structure, comparing the measured and calculated spectra show that they are not identical. This can be attributed to the different thermal and static disorder in the actual material. The Y-Sr region and high R portions of the Mo E||*aa* spectrum are noticeably shifted.

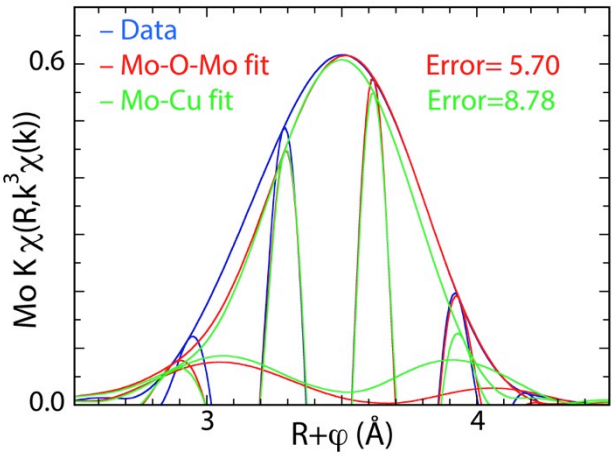

Figure S4. χ(R) of curve-fits of isolated Mo-M (M=Cu, Mo) contribution. The isolated Mo-Mo contribution, modulus and real component, are blue. It was separated from the average of the 52-78 K spectra by subtracting the contributions of all other components as calculated by the curve fit to enhance the signal:noise ratio, fitting from 3.5-14.5 $Å^{-1}$, then back transforming over this range and fitting the Fourier filtered spectrum. The red traces are the modulus, real component, and residual of the M=Mo fit with the phase and amplitude of the combined 2, 3, and 4 leg paths of the Mo-O-Mo moiety with the linear O bridge. The green traces are the modulus, real component, and residual of the fit with a Mo-Cu pair. The error was taken as the area of the modulus of the residual over this range. Using three parameters (distance, number, and Debye-Waller factor) and fifteen degrees of freedom[14] the 1.54 ratio of the error with Mo-Cu to the error of Mo-O-Mo gives a likelihood of the Mo-Cu fit relative to Mo-O-Mo as <0.01[15].

Two-site Cu2-Oap distribution. An additional finding is that the Cu2-Oap pair resides in a two-site distribution similar to that found by EXAFS in the other cuprates that have been studied[46-51], with its absence in diffraction resulting from it being a tunneling polaron. In contrast to a conventional polaron that transfers its excess charge and lattice distortion to a neighboring site by hopping, a tunneling polaron is a set of atoms that oscillate between two conformations denoted by distinct geometries and charge distributions that in chemical terms would involve changes the valence and speciation of the affected atoms[8, 16-18]. This is seen directly by subtracting the waves from the other components of the structure from the full spectrum (Fig. S5), with this procedure evaluated in the **Capabilities and limitations of EXAFS** section. The 0.28 Å separation between the Cu1-Oap and Cu2-Oap distances is 2-1/2 times as large as the 0.11 Å resolution limit derived from the maximum energy of the data k_{max}=14.7 Å^{-1}, demonstrating that the frequencies from the two shells do not overlap. The overlap in χ(R) of the Cu1-Oap and Cu2-Oap waves as an artifact of the finite range of the data that does not affect their separability has been discussed. Curve-fits identify two O positions at 2.06 and 2.22 Å, still 1-1/2 times the resolution limit of the data. The oscillatory exchange between the two conformations of the tunneling polarons would be facilitated by the cooperative action of a large number of atoms constituting a domain within a crystal where clustering of defects or substitutional atoms may already have caused the composition to differ from the bulk[19, 20]. Although the location of the double well potential in the Cu2-Oap bond is the same as for La_2CuO_{4+d} and Tl-cuprates, in YBCO it was associated with the Cu1-Oap bond. The 0.16 Å separation between the two sites in YSCO-Mo is quite close to these others despite its unusually short Cu2-Oap distance. The quality of the fit indicates that all of the O are found at one of these two positions. The Cu2-Oap double well therefore occurs for both Cu1 and Mo being the cation on its far side.

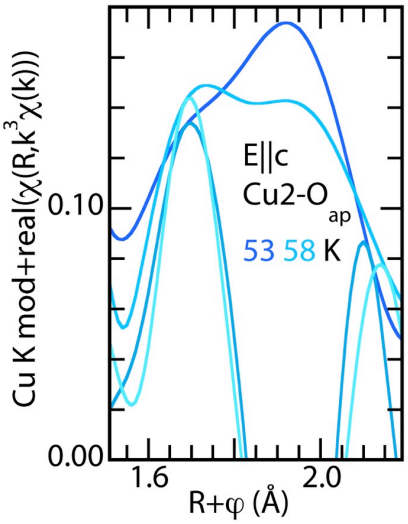

Figure S5. Cu2-Oap contribution (Fourier transform or χ(R) representation, modulus and real component) for E||*c* direction of YSCO-Mo derived by subtracting the Cu-O, Cu-Sr, and Cu-Cu contributions from the total spectrum.

XANES. The Cu and Mo valences are probed by their X-ray Absorption Near Edge Structure (XANES) that are interpreted by direct comparison with the spectra from relevant standards. For the Cu (Fig 1b in main text), the peak at 8997.5 eV and additional shoulders on the absorption edge in the E||*aa* (*a=b* in the tetragonal structure) spectrum, lower amplitude peak at 8998 eV and prominent shoulder at 8993 eV in the E||*c* YBCO spectra are typical of oriented cuprates. The Cu XANES of YBCO-Mo differ significantly from from those of closely related YBCO and other cuprates[21-23] as well as Cu_2O, CuO, and $NaCuO_2$[24]. Their spectral shapes may somewhat resemble but still differ from the XANES of molecular Cu complexes and underdoped $Bi_2Sr_2CuO_{6+\delta}$[23]. Since the local geometry is a major determinant of the XANES, this difference is inconsistent with the EXAFS that (see main text) shows that both the Cu sites closely resemble those of YBCO. The forbidden 1s→3*d* feature at 8980 eV is unusually strong. Since the amplitude of this feature is related to the number of unoccupied states[25, 26], its presence indicates that at least a fraction of the extra hole density resides on the Cu ions[2] in both *xy* and *z* types of states. A similarity with the YBCO spectrum is that the energy at the central point is higher for the E||*aa* than the E||*c* spectra. This difference is larger for YSCO-Mo than YBCO because of the substantially higher the energy of the principal absorption edge of its E||*aa* spectrum. This could result from a higher charge on the Cu in YSCO-Mo relative to YBCO since the binding energy increases with increasing charge on the absorbing atom. Alternatively, the shoulder in this region has been assigned to a 1s→4$p\pi^*$ transition involving a shakedown electron transfer from the O ions[21]. Greater hole density on the O and the resulting reduction in its number of electrons would reduce the amplitude of this feature to cause the apparent shift. Both explanations indicate a greater overall charge of the system.

A critical issue is the Mo charge that can extend to +6 compared to +3 for Cu, since that determines the charge on the Cu after subtraction from the O stoichiometry. The energies of the Mo absorption edge of the (main text Fig.1b) overlap with those of MoO_3 and are higher than for the MoO_2, demonstrating that the Mo valence is (VI)[27]. This difference in the shape of the spectrum from other Mo compounds with O[28] may result from the highly unusual Mo coordination environment found by the EXAFS and is more consistent with the highly oxidized Cu. An additional property of the XANES is that in MoO_3 the forbidden 1*s*→4*d* transition at 20008 eV is augmented by terminal, multiply bound, non-bridging O neighbors[29, 30]. The MoO_3 spectrum exhibits the greatest amplitude of this feature along the plane of these pairs for MoO_3 that contains a terminal O with Mo-O=1.69 Å and bridging O with Mo-O =1.74 Å. The MoO_2 spectrum does not show this feature. Its minimal amplitude for YSCO-Mo indicates a much more symmetric geometry than MoO_3.

XRD analysis of YSCO-Mo Cu samples. Pole figures and Rietveld analysis using the March and Dollase[31] to model the crystallite orientation.

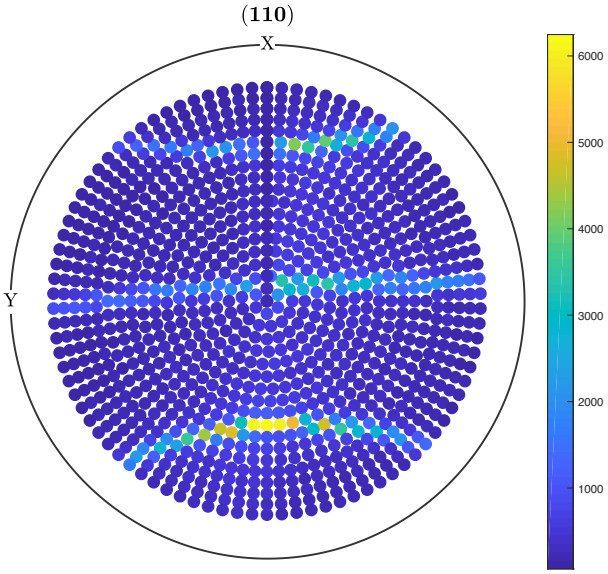

Figures S6. Cu-H sample: pole figure of 110 direction with no defocussing correction (raw data). The applied magnetic field H is perpendicular to the long axis of sample and in the diffraction plane defined by the impinging and diffracted x-ray beam. This pole figure confirms the fiber-like distribution of reflections assessing a cylindrical symmetry for the E vector distribution. This geometry allows the use of the March and Dollase model to estimate the extent of orientation.

Table S1. Results for refinement of $YSr_2Cu_{2.75}Mo_{0.25}O_{7.54}$ H||c sample:

Space group name P 4/m m m

Space group number 123

Setting number 1

Lattice parameters

a	b	c	alpha	beta	gamma
3.81700	3.81700	11.46000	90.0000	90.0000	90.0000

Unit-cell volume = 166.966337 Å^3

Structure parameters

			x	y	z	Occ.	U	Site	Sym.
1	Cu	Cu1	0.00000	0.00000	0.00000	0.750	0.000	1a	4/mmm
2	Mo	Mo1	0.00000	0.00000	0.00000	0.250	0.000	1a	4/mmm
3	Cu	Cu2	0.00000	0.00000	0.35030	1.000	0.000	2g	4mm
4	Sr	Sr1	0.50000	0.50000	0.18600	1.000	0.000	2h	4mm
5	Y	Y1	0.50000	0.50000	0.50000	1.000	1.000	1d	4/mmm
6	O	O1	0.00000	0.00000	0.16300	1.000	0.000	2g	4mm
7	O	O2	0.50000	0.00000	0.37030	1.000	0.000	4i	2mm .
8	O	O3	0.50000	0.16000	0.00000	0.390	0.001	4n	m2m .

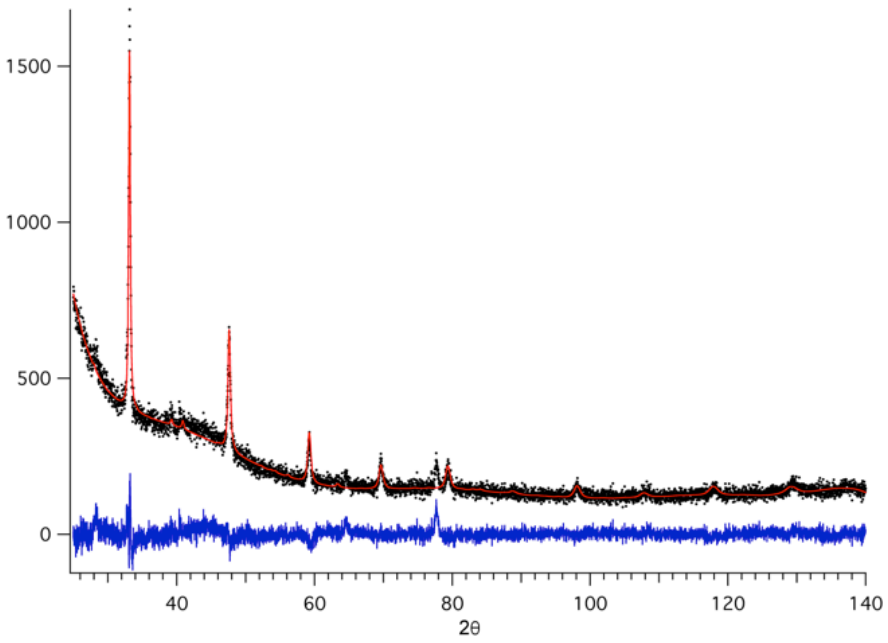

Figures S7. Cu-H Bragg –Brentano scan. Observed (dots), calculated (red) difference plot (blue). The peak at 77.5 is from the sample holder.

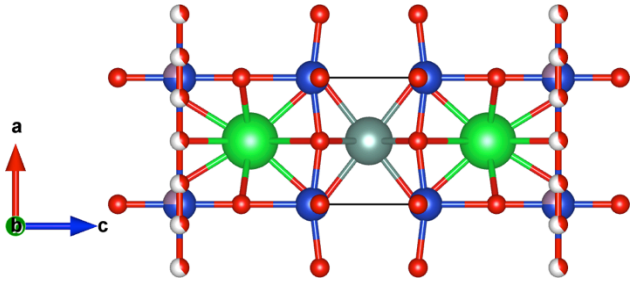

Figure S8. YSCO-Mo structure model used in the refinement.Thermal displacement parameters and atomic positions were not refined. Literature structure was used, only the March- **Dollase**[31] parameter R was refined. Rwp= 8.29%; GoF = 1.19; R_Bragg=6.56%

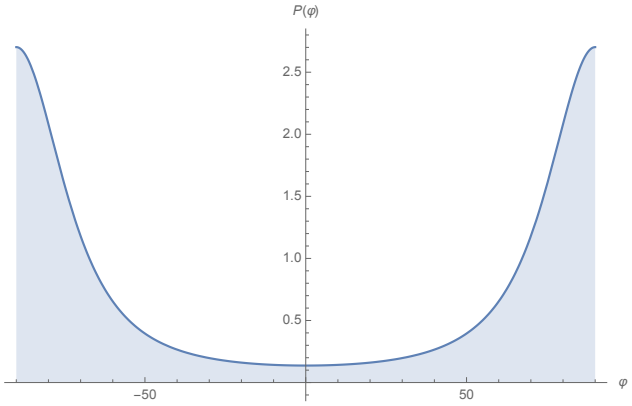

Figure S9. Actual probability function from the March & Dollase model (R=1.94(3)) obtained by the refinement of the diffraction pattern of $YSr_2Cu_{2.75}Mo_{0.25}O_{7.54}$ H||c sample. Here φ is the angle formed by the c-axes of the crystallites in the sample and the normal to the face of the sample shined by x-rays. In this case, the c-axes of the crystallites of the sample cluster along the directions parallel to the sample surface, that is the expected effect of the magnetic field.

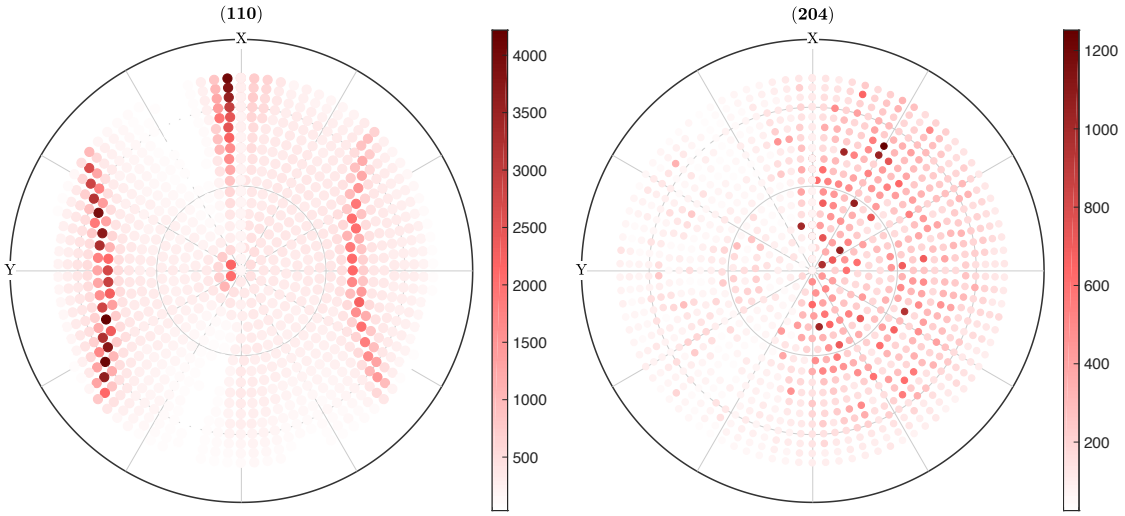

Figures S10. Cu-V sample pole figure of 110 and 204 directions No defocussing correction (raw data). The applied magnetic field H is now aligned with the long axis of sample and still in the diffraction plane defined by the impinging and outgoing beam. The 110 pole figure shows this time the E vector distribution is normal to the long axis of the sample, as expected.

References

1. A. Gauzzi, et al. Bulk superconductivity at 84 K in the strongly overdoped regime of cuprates. *Phys. Rev. B* **94**, 180509 (2016).
2. I. Grigoraviciute, et al. Electronic Structures, Hole-Doping, and Superconductivity of the s=1, 2, 3, and 4 Members of the (Cu,Mo)-12s2 Homologous Series of Superconductive Copper Oxides. *J. Am. Chem. Soc.* **132**, 838 (2010).
3. S. D. Conradson, et al. Local Lattice Distortions and Dynamics in Overdoped $YSr_2Cu_{2.75}Mo_{0.25}O_{7.54}$. *Proc. Natl. Acad. Sci. U.S.A.* this paper (2020).
4. S. D. Conradson, et al. Local Structure of $Sr_2CuO_{3.3}$, a 95 K Cuprate Superconductor without CuO_2 Planes. *Proc. Natl. Acad. Sci. U.S.A.* **in press**, (2020).
5. S. D. Conradson and I. D. Raistrick. The axial oxygen and superconductivity in $YBa_2Cu_3O_7$. *Science* **243**, 1340 (1989).
6. J. M. Deleon, et al. Planar oxygen-centered lattice instabilities in Tl-based high-temperature superconductors. *Physica C* **220**, 377 (1994).
7. G. G. Li, et al. Correlated local distortions of the TlO layers in $Tl_2Ba_2CuO_y$ - an x-ray-absorption study. *Phys. Rev. B* **51**, 8564 (1995).
8. J. M. DeLeon, et al., in *Applications of Synchrotron Radiation Techniques to Materials Science III* Vol. 437 *Materials Research Society Symposium Proceedings*, L. J. Terminello, S. M. Mini, H. Ade and D. L. Perry, Eds. (1996), (Cambridge University Press), pp. 189.
9. S. D. Conradson, J. M. DeLeon, and A. R. Bishop. Local phase separation in Tl-based oxide superconductors. *J. Supercond.* **10**, 329 (1997).
10. M. Acosta-Alejandro, J. M. de Leon, S. D. Conradson, and A. R. Bishop. Evidence for a local structural change in $La_2CuO_{4.1}$ across the superconducting transition. *J. Supercond.* **15**, 355 (2002).
11. S. D. Conradson, et al. Nanoscale heterogeneity, premartensitic nucleation, and a new plutonium structure in metastable delta fcc Pu-Ga alloys. *Phys. Rev. B* **89**, (2014).
12. D. Haskel, et al. Altered Sr environment in $La_{2-x}Sr_xCuO_4$. *Phys. Rev. B* **56**, R521 (1997).
13. J. J. Rehr, et al. Parameter-free calculations of X-ray spectra with FEFF9. *Phys. Chem. Chem. Phys.* **12**, 5503 (2010).
14. E. A. Stern. Number of relevant independent points in x-ray-absorption fine-structure spectra. *Phys. Rev. B* **48**, 9825 (1993).
15. W. C. Hamilton. Significance tests on crystallographic r factor. *Acta Crystallogr.* **18**, 502 (1965).
16. J. M. Deleon, et al. Polaron origin for anharmonicity of the axial oxygen in $YBa_2Cu_3O_7$. *Phys. Rev. Lett.* **68**, 3236 (1992).
17. M. I. Salkola, A. R. Bishop, J. M. Deleon, and S. A. Trugman. Dynamic polaron tunneling in $YBa_2Cu_3O_7$ - optical-response and inelastic neutron-scattering. *Phys. Rev. B* **49**, 3671 (1994).
18. M. I. Salkola, A. R. Bishop, S. A. Trugman, and J. M. Deleon. Correlation-function analysis of nonlinear and nonadiabatic systems - polaron tunneling. *Phys. Rev. B* **51**, 8878 (1995).
19. S. D. Conradson, et al. Possible Bose-condensate behavior in a quantum phase originating in a collective excitation in the chemically and optically doped Mott-Hubbard system UO_{2+x}. *Phys. Rev. B* **88**, (2013).
20. S. D. Conradson, et al. Possible Demonstration of a Polaronic Bose-Einstein(-Mott) Condensate in $UO_{2(+x)}$ by Ultrafast THz Spectroscopy and Microwave Dissipation. *Sci. Rep.* **5**, 15278 (2015).
21. S. M. Heald, J. M. Tranquada, A. R. Moodenbaugh, and Y. W. Xu. Orientation-dependent x-ray-absorption near-edge studies of high-T_c superconductors. *Phys. Rev. B* **38**, 761 (1988).
22. A. Bianconi, C. X. Li, S. Dellalonga, and M. Pompa. Electronic-structure of $Bi_2CaSr_2Cu_2O_8$ determined by a combined analysis of various polarized x-ray-absorption spectra. *Phys. Rev. B* **45**, 4989 (1992).
23. C. H. Chou, et al. Orientation-dependent x-ray absorption fine-structure (XAFS) of the Bi-Sr-Ca-Cu-O system. *Chin. J. Phys.* **30**, 861 (1992).
24. K. Akeyama, H. Kuroda, and N. Kosugi. Cu K-edge XANES and electronic-structure of trivalent, divalent, and monovalent Cu oxides. *Jpn. J. Appl. Phys., Part 2* **32**, 98 (1993).

25. F. de Groot, G. Vanko, and P. Glatzel. The 1s x-ray absorption pre-edge structures in transition metal oxides. *J. Phys.-Condens. Mat.* **21**, (2009).
26. R. Sarangi. X-ray absorption near-edge spectroscopy in bioinorganic chemistry: Application to M-O-2 systems. *Coord. Chem. Rev.* **257**, 459 (2013).
27. T. Ressler, J. Wienold, R. E. Jentoft, and T. Neisius. Bulk structural investigation of the reduction of MoO_3 with propene and the oxidation of MoO_2 with oxygen. *J. Catal.* **210**, 67 (2002).
28. S. Marik, et al. $Mo_xCu_{1-x}Sr_2YCu_2O_y$ (0.3 <= x <= 1) revisited: Superconductivity, magnetism and the molybdenum oxidation state. *J. Solid State Chem.* **191**, 40 (2012).
29. F. W. Kutzler, et al. Single-crystal polarized x-ray absorption-spectroscopy - observation and theory for $(MoO_2S_2)_2$. *J. Am. Chem. Soc.* **103**, 6083 (1981).
30. F. A. Lima, et al. High-resolution molybdenum K-edge X-ray absorption spectroscopy analyzed with time-dependent density functional theory. *Phys. Chem. Chem. Phys.* **15**, 20911 (2013).
31. W. A. Dollase. Correction of intensities for preferred orientation in powder diffractometry - application of the march model. *J. Appl. Crystallogr.* **19**, 267 (1986).